

# Sandpile Dynamics as a Paradigm for Turbulent Transport

D. E. Newman and B. A. Carreras

Oak Ridge National Laboratory, Oak Ridge, Tennessee 37831-8071

P. H. Diamond

University of California at San Diego, La Jolla, California 92093-0319

RECEIVED

JAN 17 1995

OSTI

"The submitted manuscript has been authored by a contractor of the U.S. Government under contract No. DE-AC05-84OR21400. Accordingly, the U.S. Government retains a nonexclusive, royalty-free license to publish or reproduce the published form of this contribution, or allow others to do so, for U.S. Government purposes."

## Abstract

To shed some light on the apparent discrepancies between most theoretical models of turbulent transport and experimental observations of the transport in magnetically confined plasmas, a model for transport<sup>1</sup> has been developed based on the concept of self-organized criticality (SOC).<sup>2</sup> This model seeks to describe the dynamics of the transport without relying on the underlying local fluctuation mechanisms. Computations based on a cellular automata model have found that SOC systems maintain average profiles that are linearly stable (submarginal) and yet are able to sustain active transport dynamics in contrast to naive marginal stability arguments. It is also found that the dominant scales in the transport dynamics in the absence of sheared flow are system scales rather than the underlying local fluctuation scales. However, the addition of sheared flow into the dynamics leads to a large reduction of the system-scale transport events and a commensurate increase in the fluctuation-scale transport events needed to maintain the constant flux. The dynamics of these models and the potential ramifications for transport studies are discussed.

## I. Introduction

A new paradigm for turbulent transport<sup>1</sup> has been suggested to shed some light on the discrepancies between predictions based on local turbulent transport theory and experimental observations. This new paradigm is based on the concept of self-organized criticality (SOC).<sup>2,3,4</sup> This concept seeks to describe the general properties of the dynamics of the transport without relying on the underlying local transport/fluctuation mechanisms. The simplest example of such a system is a sandpile model. It has been found that such SOC systems maintain average profiles that are linearly stable (submarginal) and yet are able to sustain active transport dynamics in contrast to standard marginal stability arguments. It is also found that the dominant scales in the transport dynamics are system scales rather than the underlying local fluctuation scales. In addition to allowing the paradigmatic investigation of turbulent transport, the introduction of sheared flow (wind), which arises in the context of magnetically confined plasmas, acts as a novel and important extension to their chaotic dynamics.

The dynamics of such systems can be computationally investigated with a cellular automata model of "running sandpile" dynamics. This model allows us to investigate the major dynamical scales and the effect of an applied sheared flow on these dominant scales.

The importance of this model lies in investigating two of the difficulties standing in the way of understanding anomalous transport in magnetically confined plasmas, the stability problem and the scale problem. It has long been thought that some linear instability is driving turbulent fluctuations, which are causing the anomalous transport.<sup>5</sup> A number of modes have been put forward as candidates for dominating transport in magnetic confinement devices. In many of these modes a linear marginal stability condition has been assumed for the profile. This is based on the assumption that the turbulent system would relax its driving gradient back to the linearly least unstable profile (the marginal profile) just allowing for the drive to continue. Ballooning modes

**DISCLAIMER**

**Portions of this document may be illegible  
in electronic image products. Images are  
produced from the best available original  
document.**

near the  $\beta$  limit<sup>6</sup> are among the modes for which this has been suggested. In addition, ion temperature-gradient-driven modes at the marginal limit have been suggested as the dominant core transport mechanism,<sup>7,8</sup> Unfortunately, all of these modes suffer from the drawback that experimentally the profiles seem to be stable to the candidate modes over much if not all of the radius.<sup>9</sup> The second difficulty is related to the fact that the transport from most of these modes is governed by the fluctuation scales, which is typically on the order of ion gyro radii (Gyro-Bohm scaling).<sup>10</sup> These fluctuation scales define the characteristic "step size" of the turbulent diffusion leading to a confinement time that scales with the step size. Once again the experimental evidence is that the confinement in real magnetic confinement devices, at least in the low confinement mode (L-mode), scales with the machine size (Bohm scaling).<sup>10</sup> Interestingly, there is evidence that in the enhanced confinement modes (H mode, etc.), which have a sheared flow coincident with the transport barrier, the confinement scaling seems to go from Bohm-like to Gyro-Bohm-like.<sup>11</sup>

Counter to much intuition, it is found that robust transport dominated by system-scale transport events can occur even with a profile that is on average substantially submarginal. However, the addition of sheared flow into the dynamics leads to a large reduction of the system-scale transport and a commensurate increase in the fluctuation-scale transport. This may be consistent with the transition from Bohm to Gyro-Bohm scaling observed in improved confinement modes.

The remainder of the paper is organized as follows: Section II contains the SOC model investigated and the results from unshaped simulations. This is followed by Section III, consisting of the results due to the addition of shear to the SOC system. Finally, Section IV is the conclusion and summary.

## II. The running sandpile model

Because of the expense and difficulty of modeling large regions of a magnetic confinement device and because of the difficulty of interpreting the data that does exist, it is often useful to construct the simplest model that captures the dynamics of interest. Starting from the assumptions of the importance of marginality to turbulent transport and the importance of turbulent transport to relaxation of gradients, a very simple natural model presents itself. In this model local turbulent fluctuations are excited by the local gradient exceeding marginality; the local fluctuations, in turn, relax the local gradient, transporting the excess gradient down the profile. This sandpile SOC model has the gradient modeled by the slope of the sandpile, while the turbulent transport is modeled by the local amount that falls when the sandpile becomes locally unstable. The system is driven by noise from the heating/fueling sources, which in the sandpile model is represented by a random "rain" of sand grains on the pile. This model allows us to study the dynamics of the transport independent of the local instability mechanism and independent of the local transport mechanism. Because of the relative simplicity of the model, we are also able to do very long time simulations and collect reasonably large statistical samples.

A standard cellular automata algorithm<sup>12</sup> is used to study the dynamics of the driven sandpile. The domain is divided into cells that are evolved in steps. First, "sand grains" are added to the cells with a probability  $p_0$ . Next, all the cells are checked for stability against a simple stability rule and either flagged as stable or not; finally, the cells are time advanced, with the unstable cells over

turning and moving their excess “grains” to another cell with the size, distance, and direction of the fall being determined by the overturning rule. The simplest set of rules used are as follows:

If

$$Z_n \geq Z_{crit} ,$$

$$h_n = h_n - N_f$$

and

$$h_{n+1} = h_{n+1} + N_f$$

With  $h_n$  defined as the height of cell  $n$ ,  $Z_n$  being the difference between  $h_n$  and  $h_{n+1}$ ,  $Z_{crit}$  is the critical gradient and  $N_f$  is the amount of “sand” that falls in an overturning event (Fig. 1). In terms of the usual physical quantities associate with turbulent systems,  $Z_{crit}$  is the critical gradient at which fluctuations are unstable and grow, while  $N_f$  is the amount of “gradient” that is transported by a local fluctuation (eddy turnover, for example).

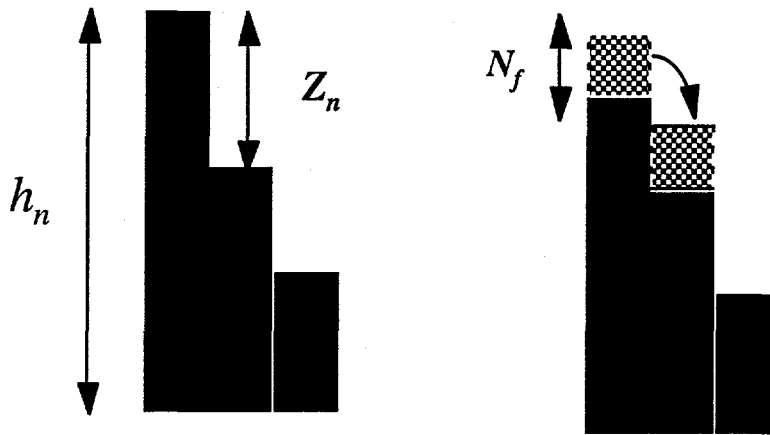


Fig. 1 A cartoon representation of the rules governing the sandpile dynamics.

The simulations are done with a variety of domain sizes varying from 50 by 1 ( $x$  and  $y$ , or  $r$  and  $\theta$  directions) to 800 by 100 with most of the two-dimensional (2-D) runs being performed at 200 by 50. The boundary conditions for the computation domain are periodic in the  $y$  direction, open at  $x = L$  (particles that reach the edge are lost), and closed at  $x = 0$ . Computations are typically started from a marginal state (i.e.  $Z_n = Z_{crit} - 1$ ) and allowed to relax to the SOC state. The relaxation time is a function of  $L$ ,  $p_0$ , and  $N_f$ . For  $L = 200$  and typical values of  $p_0$ ,  $N_f$ , this relaxation time is around 40,000 time steps. To accumulate sufficient statistics, the system is iterated for  $10^5$  to  $10^7$  time steps after saturation is reached. The main diagnostic for the sandpile model avalanche dynamics is the time history of the number of flips (overturning events), with both the total number in the system and the number for flips for individual  $y$  values tracked. Additionally, local and poloidally averaged particle fluxes are tracked at a few radial positions. Finally, the evolution of the total mass (the sum of all the grains in the system) and the profiles is followed.

To provide control results with which to compare computations with shear, we have reproduced the previously published sandpile computations<sup>2,3</sup> with shear-free running sandpiles. Because the model only has four parameters,  $L$ ,  $p_0L$ ,  $N_f$ , and  $Z_{crit}$ , we have performed scans of each of these parameters, keeping the others fixed. The results of these scans are summarized below after a review of the results from a “typical” case. Let us consider a case with  $L = 200$ ,  $p_0 = 0.0025$ ,

$N_f = 3$  and  $Z_{crit} = 8$ . Starting from a marginally stable profile ( $Z = 7$ ), the sandpile evolves for  $10^5$  time steps and reaches a steady state regime with the characteristic SOC profile. The relaxation from the marginal profile to the SOC profile can be seen (Fig. 2) in the time evolution of the number of overturning sites (flips). The SOC state is not reached until the average level of the number of flips saturates at  $\sim 20,000$  time steps.

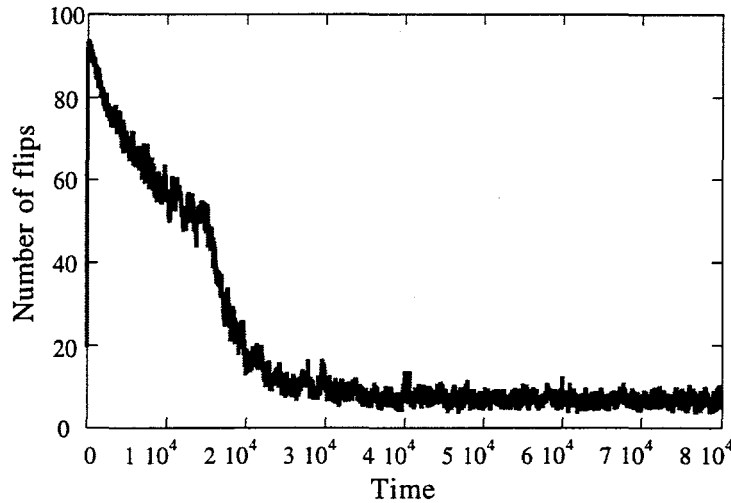


Fig. 2 Time history of the instantaneous number of overturning events (flips) showing relaxation from marginal profile to SOC profile.

The relaxation time, defined as the time to relax from marginal to the final stationary state, scales as  $L^2$  (Fig. 3). This scaling is consistent with the number of steps needed to move a distance  $L$  in a standard random walk diffusion process.

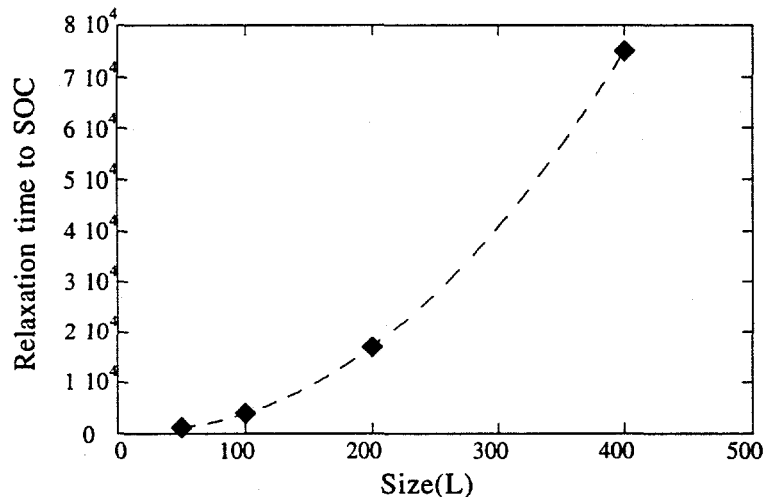


Fig. 3 Time to relax from marginal profile to final SOC profile as function of system size. All other parameters were kept constant.

Figure 4(a) shows the marginal profile and the average SOC profile (averaged over the last 20,000 steps). It can be readily seen from the slope of the SOC profile and the number of flips occurring after relaxation into SOC state that even with a significantly submarginal profile the system is able

to robustly transport the inputted flux. This is an important characteristic of SOC systems and should lead to a reexamination of the relevance of some of the modes discounted because the profiles are submarginal.

The slope,  $s = dh/dx$ , of the sandpile, while not constant with position [Fig. 4(b)], can be usefully parameterized as constant. The functional form is approximately  $s = [a - b \ln(x)] (p_0 L)^\alpha$  with  $a \approx 7 - 0.6 N_f$ ,  $b \approx 0.004 + 0.05 N_f$ , and  $\alpha$  small ( $\ll 1$ ). This functional form will be discussed in a later paper.

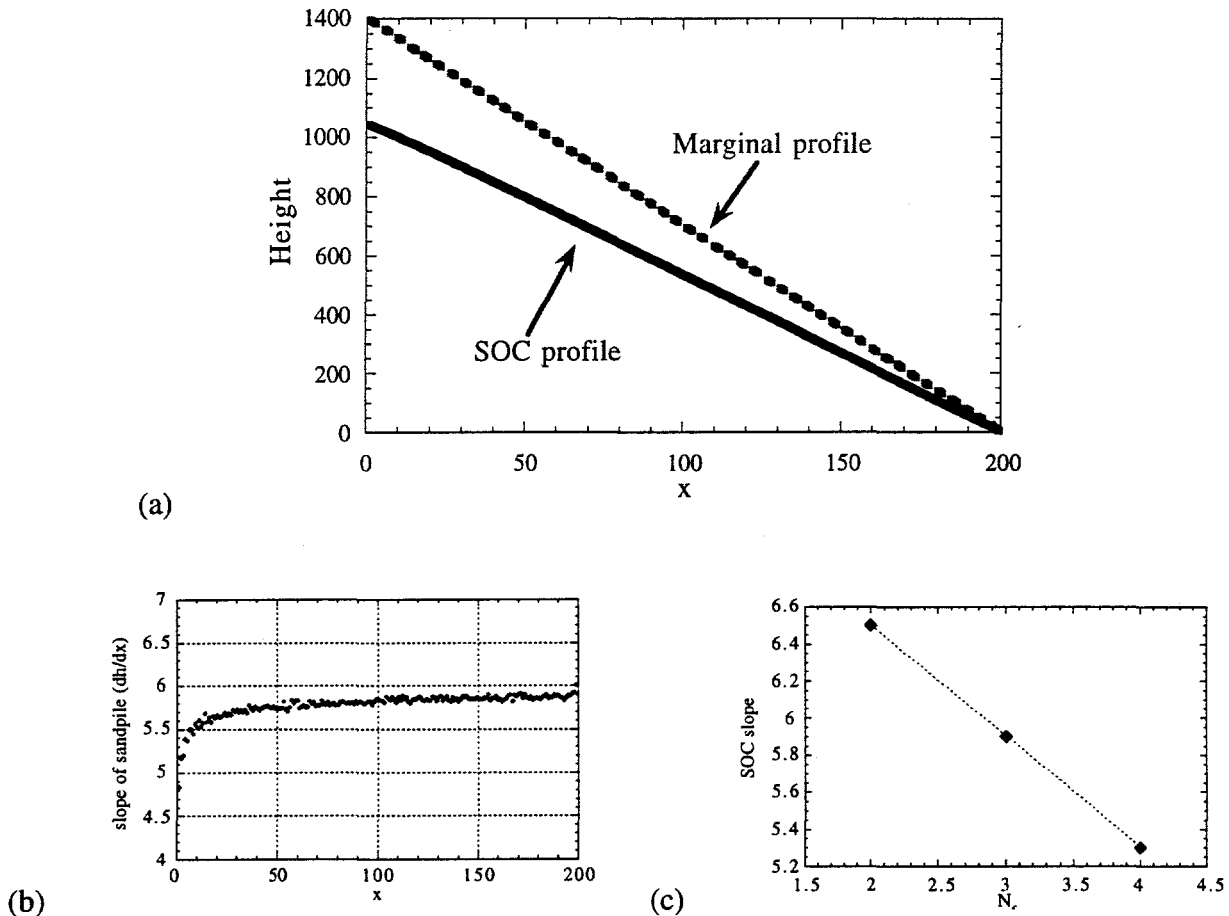


Fig. 4(a) Average sandpile profiles for case with  $N_f = 1$  (marginal case) and  $N_f = 3$  (SOC case) with all other parameters the same; (b) slope of SOC profile; (c) SOC slope as function of  $N_f$ .

The one condition needed for the maintenance of a subcritical SOC profile rather than a marginal profile is that  $N_f > 1$ . This is equivalent to saying that a turbulent eddy will attempt to transport enough to level, or partially level, the local gradient in one eddy turnover (Fig. 5).

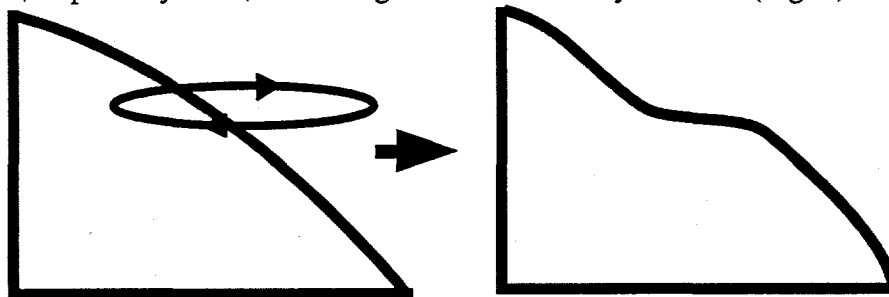


Fig. 5 Schematic representation of eddy flattening gradient in one turnover time.

If  $N_f = 1$  then whenever a sand grain is dropped onto the pile, it will fall all the way down to the bottom of the pile and exit at the base. This fall is not an organized (spatially extended) avalanche in the sense that it will not grow as it cascades down the pile because only the local cell with the extra grain is unstable (supermarginal).

A time history of overturning sites in a marginal system ( $N_f = 1$ ) vs a time history of overturning sites in our prototypical SOC case ( $N_f = 3$ ) clearly shows this difference. In the marginal case [Fig. 6(a)] all of the falls are individual isolated events (except for the places where two sand grains were dropped by chance in neighboring cells), while in the SOC case [Fig. 6(b)] coherent avalanches of all different lengths clearly exist. These figures are time slices of a given poloidal location with all the poloidal positions giving statistically the same result. The black cells are cells that are overturning at that time step while the white cells are stable.

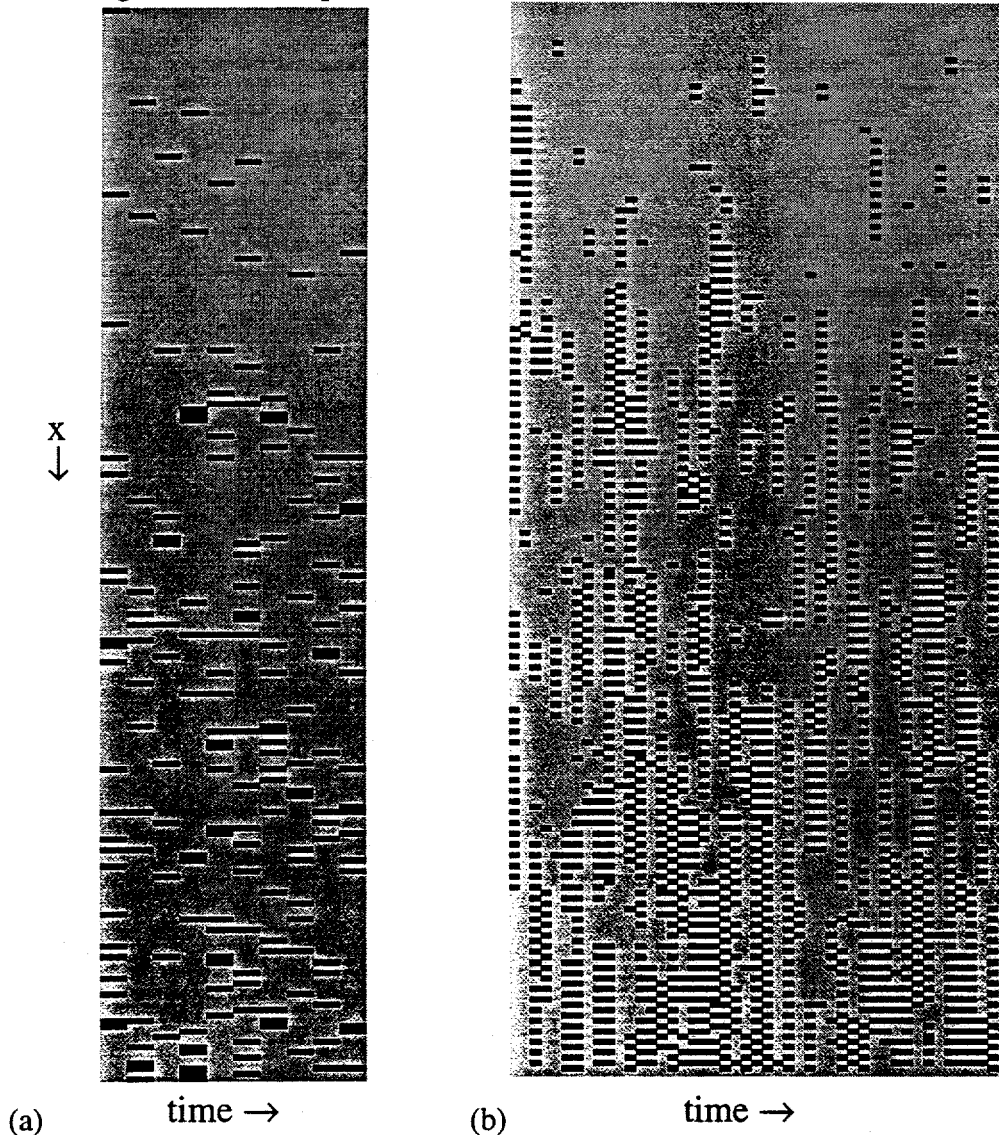


Fig. 6 Time histories of overturning sites: (a) case with  $N_f = 1$  with no “organized avalanches, and (b) avalanches of all different lengths.

To quantify the distribution of these avalanche events that typify the transport dynamics of the flowing sandpile we analyze the avalanches in two different ways. First and most simply, we construct the probability distribution function (PDF) for the total number of instantaneous flips (overturning event) (Fig. 7). For the marginal case the PDF [Fig. 7(a)] has a mean of  $p_0 L^2/2$ ,

which is the number of grains dropped at a given time step ( $p_0L$ ) times the average amount of time for a grain to leave the system ( $L/2$  if one grain moves one cell in one time step). The width ( $\langle \text{variance} \rangle^{1/2}$ ) of this PDF is just a function of the random rain rate and the distribution of the rain in  $x$  (this is normally a flat distribution). The PDFs for the SOC [Fig. 7(b)] cases also have means given by the flux into the system,  $p_0L$ , times the average time for the grains to leave the system,  $L/2$ , weighted with the amount transported in one flip,  $N_f$ , giving a mean of  $p_0L^2/2N_f$ .

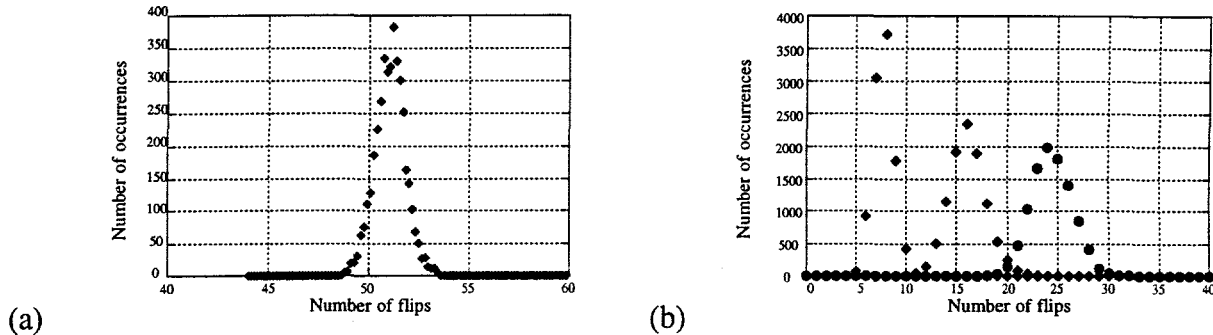


Fig. 7 Probability distribution functions (PDFs) of the flips (a) for a case with  $N_f = 1$  (marginal) and (b) for 3 different values of  $p_0$  with  $N_f = 3$ .

The variance for the SOC cases seems to scale with the mean as one would expect from a Poisson distribution,  $\text{var} \sim p_0L^2/2N_f$ . The details of the width and subtle corrections to the functional form will be dealt with in another paper because for our purposes the phenomenology of the width is sufficient.

The second method for quantifying the avalanche dynamics is with frequency diagnostics applied to time history of instantaneous flips (only using the saturated region). Figure 8 shows a typical spectrum that can be divided into three regions following Hwa et al.<sup>3</sup>

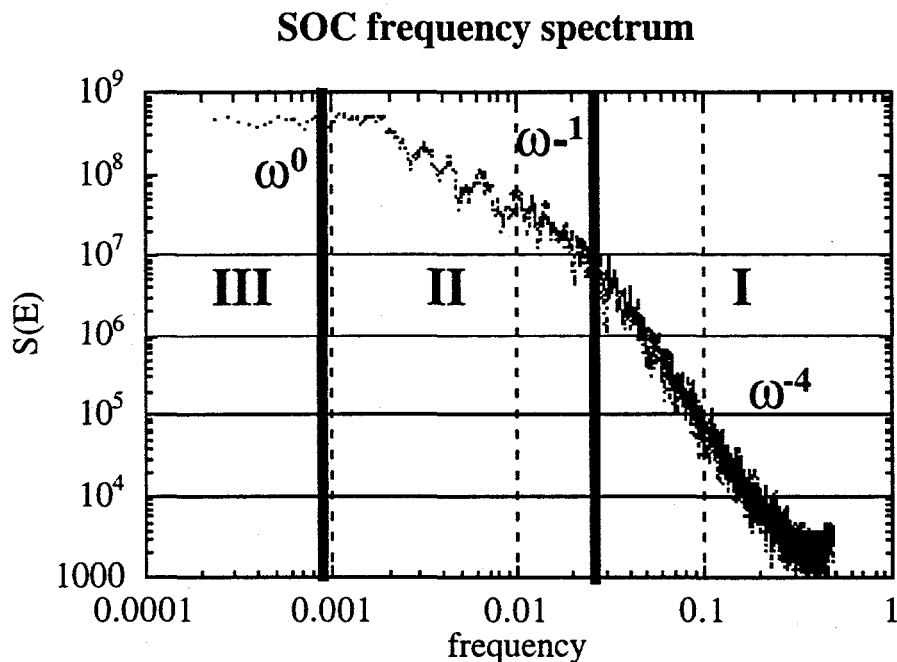


Fig. 8 Frequency spectrum of flips showing three dynamical regions typical of running sandpile.

The first region is the high-frequency end of the spectrum that follows approximately an  $\omega^{-4}$  power law. This region is identified as the noninteracting (or overlapping) avalanche region; if  $p_0$  is made small enough this region completely envelops region II (middle to low frequencies), which is identified as the overlapping avalanche region. The spectral falloff in the overlapping region is  $\sim \omega^{-1}$  and is the region of primary interest to us. Finally, there is region III, the region of lowest frequencies. In this region the spectral power is relatively flat and finally rolls over at the lowest frequencies. This region is identified with global discharge events that have extremely long correlation times. It is easiest to see these discharge events by looking at the time history of the total mass (the integrated heights). Figure 9 shows the total mass in a case that was run for  $10^7$  time steps and encompasses perhaps two of the largest “global discharge events.” Note that the frequency of these largest events is proportional to the rain rate (the input flux) as one would expect for relaxation type oscillations because the rate of refilling of the pile after a massive discharge is proportional to the input flux. Region III is a dynamically very interesting regime and is the region of primary interest to those using SOC models to study earthquakes. However, because this region involves time scales probably much longer than a confinement time (which is on the order of  $L^2$  assuming transport goes one fluctuation size in one time step), we will only explore the high-frequency end of this region .

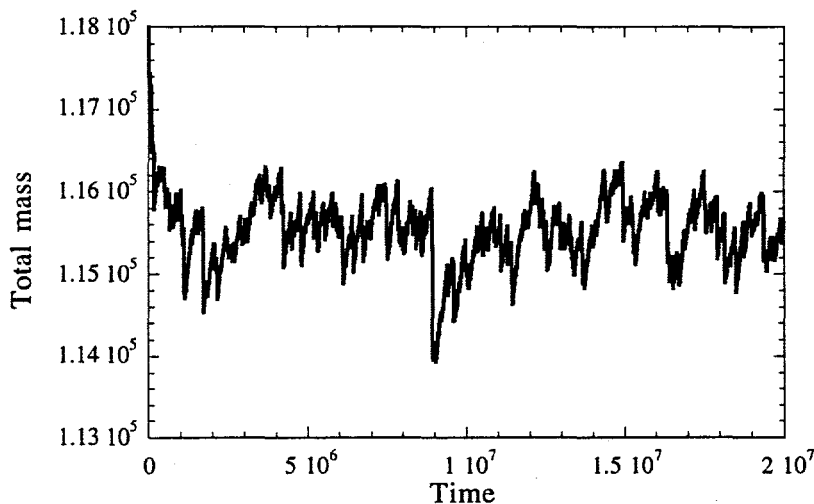


Fig. 9 Time history of the mass of sandpile showing one or two large discharge events.

To compare these cellular automata model results with analytic results<sup>1</sup> we also construct a diffusion coefficient  $D_0$  in the typical fashion from the average local flux and average local gradient, giving  $D_0 = \langle \Gamma \rangle / \langle dh/dx \rangle$ . However, since the system is in steady state, the average local flux through  $x_0$  is simply the average number of grains falling into the region above  $x_0$ , which is given by  $p_0 x_0$ . This then allows us to write  $D_0$  as  $D_0 = p_0 x_0 / \langle dh/dx \rangle$ . It is found that  $\langle dh/dx \rangle$  scales with  $p_0 x_0$ , allowing a natural way to look at the diffusion by plotting  $D_0$  vs  $p_0 x_0$ , which is done in

Fig. 10. It is found that  $D_0$  has a functional dependence of  $(p_0x)^\beta$  with  $\beta \approx 0.95$  in the region that  $p_0x$  is less than  $N_f/2$ .

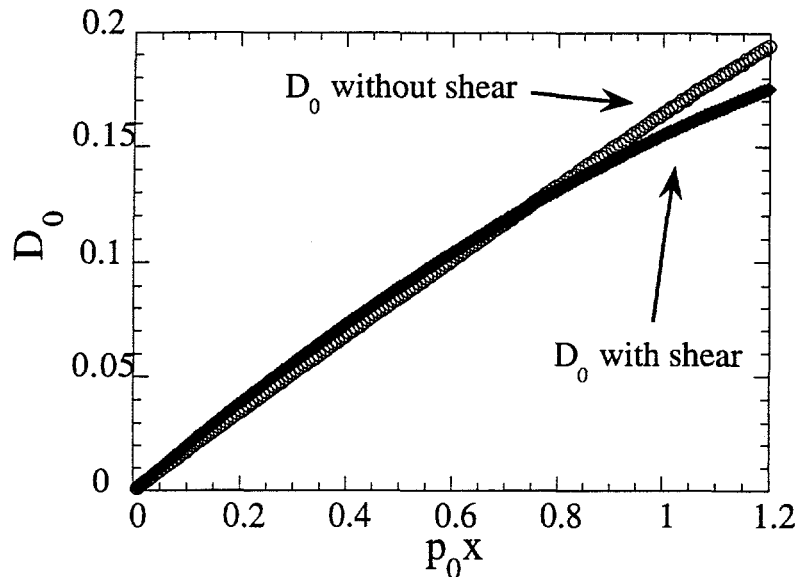


Fig. 10  $D_0$  as function of  $p_0x$  for case without shear and case with shear. Note the different functional forms.

### III. Sheared SOC model

Due in part to the existence of a flow shear region coincident with the transport barrier in enhanced confinement modes, there has been much interest recently in the effect of sheared flows on turbulent systems. This interaction can take a number of forms. The first and most often quoted is the shear suppression of the turbulence.<sup>13</sup> This occurs when the shear scale length is less than the turbulent scale length of interest and the shear rate is higher than the eddy turnover rate. In this case the turbulent fluctuations are decorrelated by the shear more quickly than they would be by the turbulent interactions; consequently, the turbulent amplitude and scale lengths are reduced. Another and sometimes more important impact of the shear flow on the fluctuation amplitude is at the linear stabilization level. This effect is mode dependent and is therefore not as general as the nonlinear shear suppression, but for the modes on which it is effective there can be a significant impact.<sup>14</sup> We will ignore the details of the local interaction between the shear and the fluctuations (both linearly and nonlinearly) and concentrate on the impact of the shear on the large-scale transport dynamics.

To use the sandpile model to study this, we now add a region of poloidal shear flow into the basic model described above. This is implemented by adding a constant poloidal flow in one direction to the top of the sandpile and a constant flow in the other direction to the bottom. The two constant flow regions are then connected by a shear flow region (Fig. 11) with a variety of possible shear profiles. The modification to the rules of the system is relatively simple and can be done in two ways (both of which have been tried). First, the local "wind" can be applied to only the falling (overturning) grains; in this case as the grain moves down (the  $x$  or  $r$  direction in our notation) the

sandpile, its position is offset in the poloidal ( $y$  or  $\theta$  direction in our notation) by an amount proportional to the local “wind speed.” Because the wind has shear, the amount of the offset varies with position. The second method involves rotating the entire sandpile so that all of the cells at a given  $x$  are moved by an amount proportional to the local wind speed at that location. In the shear region there is then differential rotation of the pile, which has the same effect as the first method. The first method is closer to the dynamics of a sand pile with a sheared wind blowing across it because only the falling particles are affected by the wind in that case. The second method is closer to the sheared flow in a turbulent magnetic confinement device because both the local gradient and the transporting quantities are advected by the sheared flow. Note that test cases were done with both methods in which there was a constant velocity wind (no shear) to make sure that the effects seen were due to the shear and not pure advection. No effect was found in the test cases.

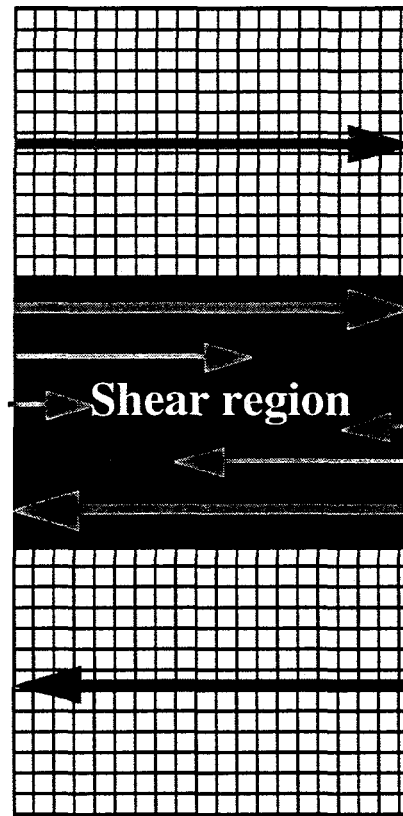


Fig. 11 Cartoon of sheared flow in sandpile model.

The poloidal flow is added to the dynamics in the time advance step after moving any falling grains to their new positions. The impact of the shear flow is quantified by changing a shear parameter made up of the product of both the magnitude of the shear and the size of the shear region.

The effect of the shear on the transport dynamics can be first and most easily observed in a time history of the overturning sites (Fig. 12). The sheared region in the middle is easily differentiated from the unsheared ends by the absence of correlated transport events (avalanches) in the shear zone. This can be contrasted to the unsheared SOC case shown in Fig. 6(b). Although the difference in avalanche dynamics is visually striking and shows clearly the decorrelation of transport events by the shear flow, to quantify the changes we must use the other diagnostics.

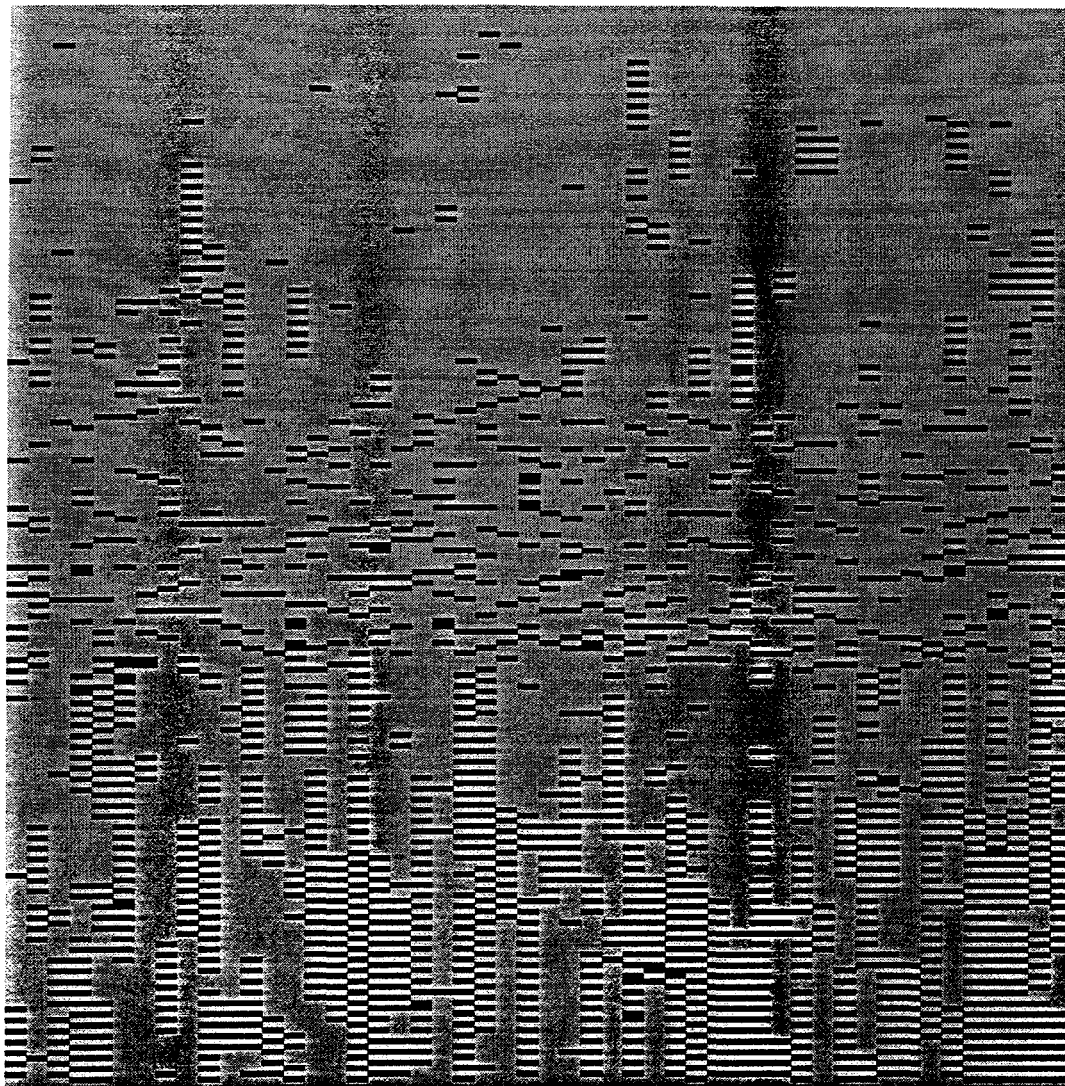


Fig. 12 Time histories of overturning sites with shear region in the middle. Decorrelation of avalanches can be seen in shear region.

Looking once again at the PDF of the flips, one can see a marked decrease in the variance for a running sandpile with shear when compared to one without shear [Fig. 13(a)]. This trend continues when the shear and size of the shear zone increases [Fig. 13(b)]. This suggests that the larger scale transport events are being suppressed by the shear, and because the total flux must remain the same, the medium- and small-scale events must increase to make up the difference.

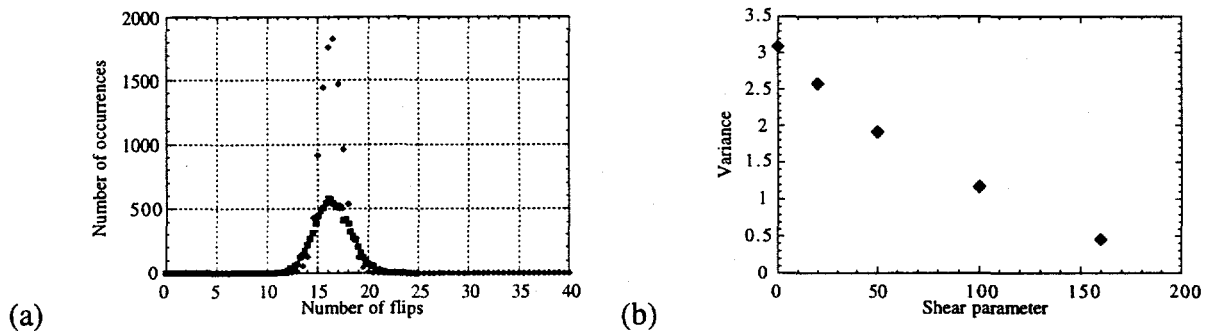


Fig. 13 PDFs for case with shear (diamonds) and without shear (squares), note narrowing of the PDF with shear; (b) the variance (the squared width) as function of shear parameter.

It should be kept in mind that the number of flips is not strictly a measure of avalanche size as three avalanches of size 5 occurring at the same time gives the same number of flips as one avalanche of size 15. Therefore, the decorrelation of the large-scale avalanches must be made up to some degree by multiple simultaneous small slides. The frequency spectra make an even more compelling case for the impact of shear on the transport dynamics of the running sandpile. By simply comparing the spectra for an unsheared case with a sheared case, one can see a suppression of the low-frequency end of the spectrum and an increase in the high-frequency end. This can be quantified through the mean frequency  $\bar{\omega}$ , defined as  $\bar{\omega} = \int \omega S(E) d\omega$ . Figure 14 shows the variation in  $\tau_d$  ( $1/\bar{\omega}$ ) as the shear parameter is increased. This shows the decorrelation time of the transport decreasing as the shear parameter increases.

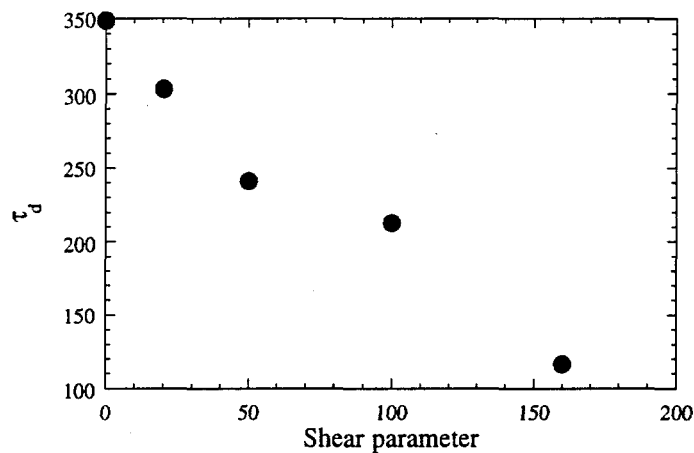


Fig. 14 Decorrelation time as function of shear parameter.

Once again it is important to note that this effect is completely different from the shear suppression of turbulence. In this model the turbulent amplitude is not being affected at all; only the correlated transport events are being modified. Therefore, this decorrelation time is not the standard turbulent decorrelation time but rather a new quantity, a transport decorrelation time. In the shear-free case the transport decorrelation time is longer than  $L^2$ , while in the sheared case the decorrelation time becomes shorter than  $L^2$ .

The next logical questions to ask are the following: if the transport events are being decorrelated, what is the impact on the diffusion coefficient, and does this build up a transport barrier? The answers to both of these questions are somewhat subtle. The diffusion coefficient  $D_{eff}$  changes functional form (Fig. 10), leading to an increase in the diffusion coefficient for small  $p_0x$  and a decrease for large  $p_0x$ . The new form is  $D_{eff} = \frac{P_0x}{a + bP_0x}$ . This change in functional form is

consistent with the change in dynamics suggested by analytic work on the Burgers equation model by Diamond and Hahm<sup>1</sup> for SOC. However, the actual functional forms disagree, which may not be surprising given that one model is continuous while the other is discrete. In the asymptotic limit

of large  $p_0x$  there is very good agreement between the model and the analytics. The analytic form of the diffusion coefficient goes from infrared divergent ( $D \propto k_r^{-1}$ ) in the shear-free case to independent of  $k_r$  ( $D \propto k_r^0$ ) in the sheared flow case with  $k_r$  being the inverse of the radial scale length  $x$ . The asymptotic limit ( $x \rightarrow \infty$ ) of the diffusion coefficients in the sand pile model show the same dependence going to a constant with shear and  $k_r^{-0.98}$  without shear. In the model as presented up to this point, the inclusion of shear can either cause a transport barrier, a steepening of the gradient with the coincident decrease in the diffusion coefficient, or an antitransport barrier in which the gradient is further reduced and the diffusion coefficient (as defined) is therefore increased. In the asymptotic limit as  $p_0x$  gets large, the diffusion coefficient becomes smaller than the unsheared case, and a transport barrier develops. The slope of the sandpile with shear is shown in Fig. 15. The shear region can be clearly seen with an increase in the slope in the shear region. It should be kept in mind that the two other effects of shear on turbulent transport, the shear suppression of turbulence and the increased stability of the mode, are not included in this model. These will be briefly dealt with later.

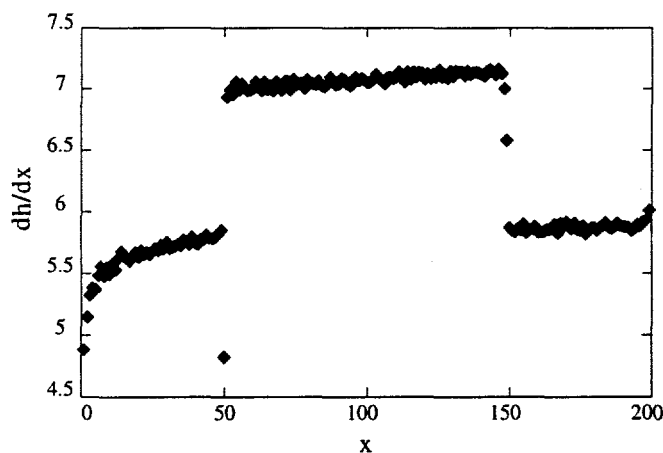


Fig. 15 Slope of sandpile with shear. The marginal slope would be 7. In regions without shear the SOC slope is less than marginal; however, in region with shear a large increase in slope can be seen.

As discussed before, sheared flow can have multiple effects on turbulent transport. In the sandpile model the overturning events are the turbulent fluctuations driving the transport. Therefore, since shear can reduce the turbulence amplitude, in the sandpile paradigm  $N_f$ , the amount moved in an overturning should be affected by the shear. Similarly, because sheared flow often has an effect on the linear stability of a mode, shear should have an impact on  $Z_{crit}$ , the marginal stability level. If we include in the sandpile model a reduction in  $N_f$  proportional to the shear and an increase in  $Z_{crit}$  also proportional to the shear, we obtain a confluence of effects on the gradient, and therefore the diffusion also, due to the shearing effects that add up to more than the sum of the individual changes (Fig. 16). The inclusion of these two additional effects is not meant to be self-consistent,

but rather a demonstration that the real impact of shear on transport is likely to be enhanced by the combination of effects.

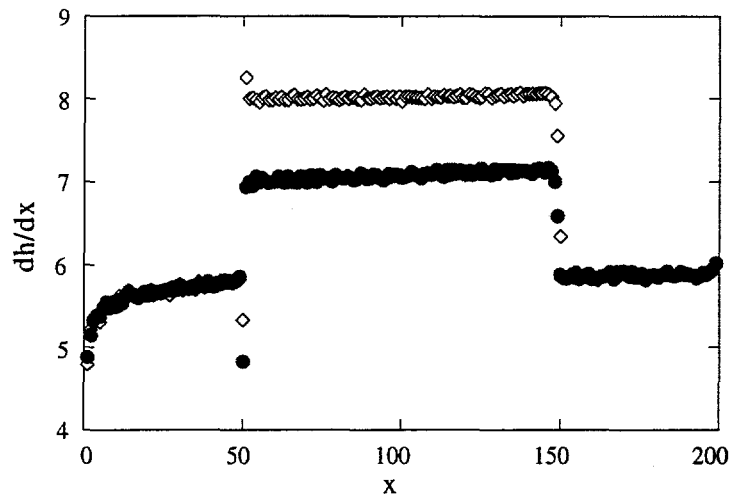


Fig. 16 Slope of sandpile with shear: one case (circles) without linear effects and the other case (diamonds) with linear effects.

#### IV. Conclusions

Within the constraints of a cellular automata model of critical gradient dynamics (the running sandpile model), the following conclusions were reached.

(1) Robust transport can occur with profiles that are on average submarginal. This may be relevant to the experimental observations that over much of the radius the profile appears to be marginal or submarginal to most of the modes suspected of dominating transport. The deviation of the average slope from marginality is proportional to the amount that gets locally transported  $N_f$ .

(2) Transport events, avalanches, are found on all size and time scales in the running system. The coherence of large transport events can make the transport scale with the system size even though the local transport mechanism is much smaller scale.

(3) The addition of sheared flow to the running sandpile has a major impact on the transport dynamics. The dominant scales seem to move from system size to smaller scales.

(4) With moderately strong driving, the inclusion of shear can cause the formation of a "transport barrier" (a region with decreased diffusivity). However, in this model, which does not include any of the standard shear effects such as linear stabilization and suppression of turbulence, very weak driving can lead to an increased diffusivity in the shear region. When the other impacts of shear are included in an ad hoc manner, the shear region always exhibits a decreased diffusivity with the coincident transport barrier.

The possibility of transport, which is largely independent of the nature of the local instability and furthermore can occur even with average gradients that are submarginal, should lead to the reevaluation of some modes that may have been discounted due to the profiles. Because the dynamics of the transport are not closely tied to the local dynamics (the instability driving the fluctuations), this type of model would suggest a universality in transport even when the instabilities are different (i.e., across machines). Shear decorrelation of transport events provides a universal mechanism by which shear can have an impact on transport without needing the details of the local instability. While it is unlikely that this decorrelation of transport events is the entire answer, it does provide interesting avenues to explore both experimentally and theoretically.

## Acknowledgments

Valuable discussions with T. S. Hahm and J.-N. Leboeuf are gratefully acknowledged. D. E. Newman would like to thank Oak Ridge National Laboratory for its support through the Wigner Fellowship Program. This work is supported by the U.S. Department of Energy under contract DE-AC05-84OR21400 with Lockheed Martin Energy Systems, Inc., and Grant No. DE-FG03-88ER-53275 with University of California, San Diego.

---

<sup>1</sup> P. H. Diamond and T. S. Hahm, On the dynamics of turbulent transport near marginal stability, in press *Physics of Plasmas*.

<sup>2</sup> P. Bak, C. Tang, and K. Wiesenfeld, *Phys. Rev. Lett.*, **59** 381 (1987).

<sup>3</sup> T. Hwa and M. Kardar, *Phys. Rev. A*, **45** 7002 (1992).

<sup>4</sup> J. M. Carlson and J. S. Langer, *Phys. Rev. Lett.*, **62**, 2632 (1989).

<sup>5</sup> P. C. Liewer, *Nucl. Fusion* **25**, 543 (1985).

<sup>6</sup> J. W. Connor, J. B. Taylor, and M. Turner, *Nucl. Fusion* **22**, 256 (1984).

<sup>7</sup> T. S. Hahm and W. M. Tang, *Phys. Fluids B* **1**, 1185 (1989).

<sup>8</sup> H. Biglari, P. H. Diamond, and M. N. Rosenbluth, *Phys. Fluids B* **1**, 109 (1989).

<sup>9</sup> G. W. Rewoldt, L. Lao, and W. M. Tang, paper 3C48 Sherwood, 1995.

<sup>10</sup> F. W. Perkins et al, *Phys. Fluids B* **5**, 477 (1993).

<sup>11</sup> T. C. Luce et al, in *Proceedings of Fifteenth International Conference on Plasma Phys. and Contr. Fus. Research*, Seville, Spain Paper A-2-111-2, (1994).

<sup>12</sup> L. P. Kadanoff, S. R. Nagel, L. Wu, and S.-M. Zhou, *Phys. Rev. A* **39**, 6524 (1989).

<sup>13</sup> H. Biglari, P. H. Diamond, and P. W. Terry, *Phys. Fluids B* **2**, 1 (1990).

<sup>14</sup> B. A. Carreras, K. Sidikman, P. H. Diamond, P. W. Terry, and L. Garcia, *Phys. Fluids B* **4**, 10 (1992).

## DISCLAIMER

This report was prepared as an account of work sponsored by an agency of the United States Government. Neither the United States Government nor any agency thereof, nor any of their employees, makes any warranty, express or implied, or assumes any legal liability or responsibility for the accuracy, completeness, or usefulness of any information, apparatus, product, or process disclosed, or represents that its use would not infringe privately owned rights. Reference herein to any specific commercial product, process, or service by trade name, trademark, manufacturer, or otherwise does not necessarily constitute or imply its endorsement, recommendation, or favoring by the United States Government or any agency thereof. The views and opinions of authors expressed herein do not necessarily state or reflect those of the United States Government or any agency thereof.